Characterization and modeling of a planar ultrasonic piezoelectric transducer for periodontal scalers

Diego Stutzer [a,b,c], Martin Hofmann [b,c], Dominik Wenger [a], Khaled Harmouch [d], Deirdré Lenoir [d], Juergen Burger [b], Thomas Niederhauser [a,b,*]

[a] *Institute for Human Centered Engineering HuCE, Bern University of Applied Sciences, Biel, Switzerland*
[b] *sitem Center for Translational Medicine and Biomedical Entrepreneurship, University of Bern, Bern, Switzerland*
[c] *Graduate School for Cellular and Biomedical Sciences, University of Bern, Bern, Switzerland*
[d] *Electro Medical Systems S.A., Nyon, Switzerland*

ARTICLE INFO

ABSTRACT

Caries and periodontitis affect the majority of adults during their lifetime. Piezoelectric ultrasonic scalers offer great benefits during the prevention and treatment of periodontal diseases. Our group developed a novel ultrasonic periodontal scaler based on a planar piezoelectric transducer. However, similar to other piezoelectric configurations, the transducer's characteristics are strongly influenced by operation conditions. In this study, we investigated the influence of driving voltage amplitude and loading force applied using physical calculus models on the novel planar transducer's input impedance and vibration. Our results show that the resonance frequency, i.e. the frequency at which maximal deflection of the tip occurs, decreases with increasing driving voltage amplitude while it increases with increasing force. Additionally, decreasing driving voltage amplitudes and increasing force both increase the minimal magnitude and reduce the maximal phase of the input impedance near resonance. Based on these observations, we developed a procedure to extend the Butterworth–Van-Dyke (BVD) Model. The extended BVD models allow to simulate the transducer in realistic scenarios and may facilitate the development of dedicated control systems for planar piezoelectric transducers.

1. Introduction

Caries and periodontal disease are widespread problems and affect most adults during their lifetime [1]. They are caused by dental biofilm and calculus formation and can impair an individual's quality of life by causing bad breath, swollen or bleeding gums, pain, or even loss of teeth or bone. Furthermore, they may increase the risk of systemic diseases and even mortality [2]. Apart from good oral hygiene, scaling by a periodontist is part of the routine prevention and treatment of periodontal disease. While manual scalers, such as curettes, are still prevalent worldwide, power-driven scalers could offer major advantages, such as reduced operator fatigue, facilitated removal of calculus and biofilm, and efficient protection of the gingiva and the teeth of the patient [3]. Contemporary systems comprise piezoelectric or magnetostrictive ultrasonic transducers, an electronic driver, and eventually a controller to adjust the driving frequency and ensure constant amplitude of vibration of the tip.

Until now, piezoelectric periodontal power-scalers are based on Langevin-style transducers. In 1994 Amit Lal et al. developed a novel concept for an ultrasonic transducer based on a planar construction [4,

5]. This concept may drastically reduce the number of components and improve the scaling performance while reducing production costs. More recently, an ultrasonic scalpel based on a planar transducer configuration has been investigated [6,7]. This transducer showed promising results concerning the vibration amplitude. However, fast mechanical load variations during cutting through tissue (e.g., pork muscle) considerably altered the transducer characteristics. Consequently, the feedback control system could not control the vibration satisfactorily, which limited the cutting ability [7] and even contributed to the breakage of the transducer [6].

In previous work, a promising planar piezoelectric transducer for use in periodontal scalers has been developed by our group [8]. Although the design and prototyping were driven by extensive finite element model simulations [9], the novel ultrasonic transducer has not been characterized under realistic operating conditions so far.

Likewise to the ultrasonic scalpel, however, detailed knowledge about the transducer's characteristics is crucial to develop an appropriate feedback control system. Moreover, a mathematical model reproducing the influence of operating conditions, such as driving voltage
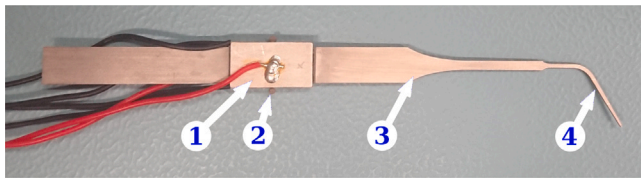

Fig. 1. Prototype of a planar ultrasonic transducer for a periodontal scaler developed by our group in previous work [8]. Two piezoelectric elements (1) are glued to a titanium sheet comprising two mounting flanges (2), a section acting as a sonotrode (3), and a tip (4).
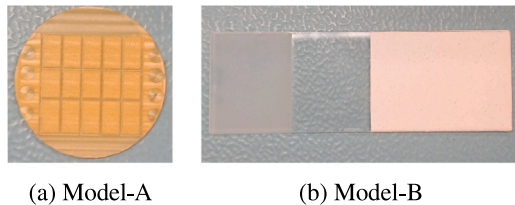

(a) Model-A   (b) Model-B

Fig. 2. Physical calculus models. Model-A (a) represents hard calculus, while Model-B (b) represents comparatively soft calculus.
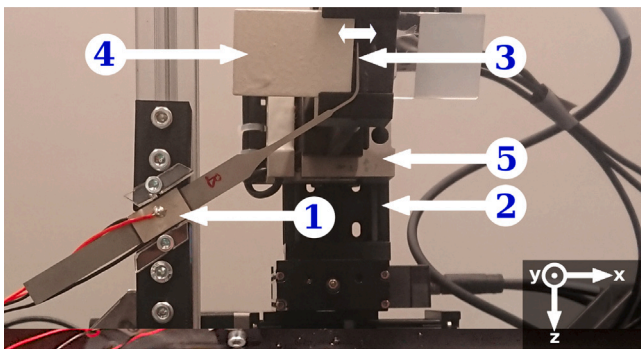

Fig. 3. Transducer (1) mounted on the measurement system. Three stepper-motor-based linear axes (2) apply a force at the tip of the transducer (3) using a physical calculus model (4) mounted on a three-axis load cell (5). The white double-arrow indicates the main axis of vibration of the tip.

amplitude and load would greatly facilitate the control design. To the author's best knowledge, such a model for planar ultrasonic transducers has not been investigated yet.

The main objective of this study was to gather fundamental knowledge required to develop performant control systems for planar ultrasonic periodontal scalers. Our goal was to investigate the electro-mechanical characteristics of the novel transducer [8] under realistic operating conditions and to derive a suitable mathematical model.

This paper is structured as follows: After an overview of relevant existing literature in Section 2, the system and concept to analyze the electro-mechanical characteristics of a planar ultrasonic transducer at varying driving voltage amplitudes and loads and to derive a mathematical model, respectively, are summarized in Section 3. The results of the measurements and the mathematical models are presented in Section 4, followed by a discussion (Section 5) and a conclusion (Section 6).

2. Literature review

2.1. Control systems for ultrasonic piezoelectric transducers

In most applications of ultrasonic transducers, feedback control systems aim to track the mechanical resonance frequency f_0 (frequency of maximal displacement) to maintain high efficiency and produce

sufficiently strong vibrations [10–14]. Moreover, the control systems try to keep the displacement amplitude $\hat{d}$ at the desired level. Since a direct measurement of the vibration is difficult or impossible to achieve in many applications, control systems can only rely on measurements of the input impedance or admittance magnitude $|Z_{in}|$ and phase $\angle Z_{in}$.

Various feedback control algorithms to achieve this task are described in scientific literature, such as phase-locked loops [12,15,16], oscillator circuits [17,18], or "hill-climbing algorithms" [19,20].

However, most algorithms are designed based on a simple linear model (see Section 2.4) of the ultrasonic transducer and consequently do not take realistic operating conditions into account.

2.2. Influence of operating conditions on ultrasonic piezoelectric transducers

Several studies [21–25] have shown that the electro-mechanical characteristics of ultrasonic transducers are strongly influenced by the driving voltage, the load material, and the magnitude of force applied to the transducer. The sensitivity to these operating conditions depends on the construction of the transducer, as well. However, detailed knowledge about this influence on transducers used in medical applications is limited and primarily based on Langevin-style transducers [21].

S. Bussier studied the influence of driving voltage amplitude on a Langevin transducer. An increasing driving voltage amplitude reduced the resonance frequency but did not measurably influence the magnitude or phase of the input impedance at resonance [25].

Ying et al. studied the influence of various tissues on an ultrasonic surgery scalpel (Exploiter™, Beyonder Co., Ltd., Beijing, China). The contact with soft tissue decreased the resonance frequency of the ultrasonic scalpel, while contact with spongy or compact bone increased the resonance frequency as compared to operation in air. Contact with tissue also increased the magnitude of the input impedance at resonance [21]. These results were also confirmed by other studies that investigated the influence of various plastic materials as well as solid and liquid loads on Langevin transducers for ultrasonic cleaning and machining [22–25].

Nevertheless, the influence of driving voltage amplitude and the influence of load acting on ultrasonic periodontal scalers, outlined in Section 2.3 in more detail, have yet to be investigated for planar piezoelectric transducers.

2.3. Load acting on ultrasonic periodontal scalers

The mechanical load acting on ultrasonic periodontal scalers changes considerably during use: The scaler's tip may be in free air or in contact with calculus, and the force applied by the operator may change during operation.

M. Ruppert et al. measured forces applied by professionals during treatment using a modified magnetostrictive ultrasonic scaler ranging from 0.2 N up to 1.34 N [26]. These results are in line with other studies, which confirm that the applied force can vary considerably [27–29].

Additionally, the mechanical properties of dental calculus can vary greatly [30–33]. In a comprehensive study, D.J. White measured the Vickers hardness of calculus on extracted teeth. Typical values ranged from 20 HV to 40 HV [31], although values of almost 0 HV up to 190 HV had also been observed.

However, the influence of contact with dental calculus on planar ultrasonic transducers has not been investigated so far.

2.4. Models for ultrasonic piezoelectric transducers

To model ultrasonic piezoelectric transducers, the so-called Butterworth–Van-Dyke (BVD) model is recommended by the IEEE standard on piezoelectricity [34] and used in many control approaches for piezoelectric transducers [14,17,35–38].
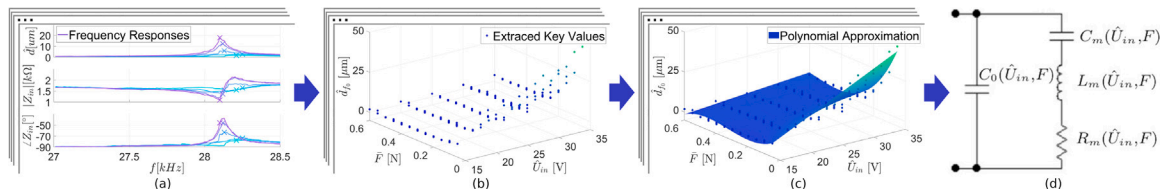
Fig. 4. Procedure to derive an extended BVD model: Frequency responses (a), as shown in Fig. 5, are analyzed to extract values of key parameters in dependence of driving voltage amplitude and force applied at the transducer's tip (b), as shown in more detail in Fig. 6. Then, the dependence of the key parameters on operating conditions is approximated by polynomials (c), as shown in Fig. 7. Finally, these approximations are used to calculate equations for the electrical equivalent circuit parameters of an extended BVD model (d), as outlined in Table 3.

The BVD model consists of four electrical equivalent circuit parameters C_0, C_m, L_m, and R_m (as depicted in Fig. 4(d)) [39–41]. The capacitance C_0 models the dielectric capacitance of the piezoelectric elements and parasitic capacitances of cables and driver electronics and dominates the impedance of the transducer at frequencies outside resonance. The coefficients C_m, L_m, and R_m model the transducer's mechanical oscillation. The capacitance C_m corresponds to the compliance of a mechanical oscillator, while the inductance L_m corresponds to the mass and the resistance R_m to the dissipation. The driving voltage represents a driving force applied to the mechanical oscillator. The current through C_m, L_m, and R_m is related to the velocity of the tip's oscillation by a coupling factor, also known as force factor in its inverse form [42], denoted by α in this paper. In its standard form, the BVD model does not reproduce the influence of operating conditions on the transducer's characteristics.

3. Materials and methods

3.1. Piezoelectric transducer

A prototype of a planar piezoelectric ultrasonic transducer for use in periodontal scalers [8,9] is depicted in Fig. 1. The transducer is based on a planar arrangement of two piezoelectric elements and a titanium sheet. The piezoelectric elements are electrically connected in parallel and driven in transverse piezoelectric mode (d_{31}) to induce a longitudinal vibration in the titanium sheet. The piezoelectric elements are made of NCE41 (CTS Corp., Albuquerque, USA) and have a size of 18 mm *x* 10 mm *x* 1 mm. They are oppositely bonded to the titanium sheet made of Ti–6Al–4V (Thyssenkrupp Materials Schweiz Ag, Bronschhofen, Switzerland) with a size of 8 mm *x* 127.8 mm *x* 1 mm (without flanges) using a high-strength epoxy adhesive (DE-LOMONOPOX GE785, DELO Industrie Klebstoffe, Windach, Germany). The titanium sheet also comprises two mounting flanges, a section acting as a vibration-amplifying sonotrode, and a tip that further enhances the vibration and facilitates supra- and sub-gingival scaling. The transducer is designed to have a resonance frequency of approximately 28 kHz.

3.2. Physical models for calculus

Two physical models were used to apply forces at the tip of the transducer.

Model-A, shown in Fig. 2(a), represents comparatively hard calculus. It was developed by E.M.S SA (Nyon, Switzerland) and consists of a mixture of ten weight parts of "Neukadur Multicast 15", twenty-three weight parts of "Neukadur Härter ISO3" (Altropol Kunststoff GmbH, Stockelsdorf, Germany), and thirty-three weight-parts CaCO3 "Omyacarb 30um" (Omya AG, Oftrigen, Switzerland) applied as a thin layer (approximately 0.05–0.1 mm) on a circular glass plate. Our measurements showed that the Vickers hardness of Model-A is 24 HV on average. Furthermore, multiple dentists consistently reported that this artificial calculus is very similar to calculus encountered in patients who did not receive professional cleaning for one or more years.

Model-B, shown in Fig. 2(b), represents comparatively soft calculus. It was also developed by E.M.S SA (Nyon, Switzerland) and consists of a mixture of ten weight-parts of "Miocolor Aqua Hartgrund Farblos" (Migros Genos-senschafts Bund, Zürich, Switzerland) and six weight parts "Krone Gips" (Hilliges Gipswerk GmbH, Osterode am Harz, Germany) applied as a thin layer (approximately 0.1–0.15 mm) on a specimen slide. Measurements showed that the Vickers hardness of Model-B is 4.6 HV on average. Dentists reported that this artificial calculus is comparable to calculus encountered during regular recalls of patients every few months.

3.3. Measurement system

A customized measurement system was developed, partially depicted in Fig. 3. The transducer (1) is mechanically mounted to the measurement system using the transducer's mounting flanges (see Fig. 1). A force of desired magnitude and direction is applied at the tip of the transducer (3) using a physical calculus model (4). The calculus model is mounted on a three-axis force sensor (5) and moved by a custom-built mechanic consisting of 3 linear axes driven by stepper motors (2) (X-XYZ-LSM025 A, Zaber Technologies Inc, Vancouver, Canada). The force components in all axes can be adjusted individually. A DAQ-Module (USB-6366, National Instruments Corp., Austin, USA) and a power amplifier ("PX200-100,100", PiezoDrive, Shortland, Australia) generate a sinusoidal voltage of adjustable amplitude and frequency to drive the transducer. The tip's vibration velocity, the driving voltage, the driving current, and the force applied at the tip are measured using a laser Doppler vibrometer (PSV-500, Polytec GmbH, Waldbronn, Germany), the three-axis force sensor (ZM3DW-AL 10N, Anhui Zhimin Electrical Technology, Bengbu, China), and corresponding electronic modules by the DAQ-Module, respectively.

The execution of the numerous individual measurements is automated using a script for MATLAB (MathWorks Inc., Natick, USA) running on a personal computer. First, a driving voltage of desired frequency and amplitude is applied to the transducer. Then, the force acting on the tip of the transducer is adjusted. Thereafter, the system waits for a settling time of 100 ms to ensure that the transducer's oscillation reaches a steady state. Subsequently, data is recorded during 30 ms. After the measurement, the amplitudes and phases of the driving voltage, the input current, and the tip's vibration are calculated by fitting sine waves of the given driving frequency to the measurements using the least squares method. Finally, the input impedance is calculated, and the sequence is repeated for another combination of operating conditions. The driving voltage frequency varied from 27 kHz to 29 kHz to cover the resonance of the transducer and nearby frequencies. The driving voltage amplitude varied between 15 Vp and 35 Vp, since voltages in this range result in sufficient vibration of the transducer. The components of the force parallel to the main axis of the tip's vibration (x-axis illustrated in Fig. 3) and perpendicular to the transducer's plane (y-axis illustrated in Fig. 3) varied between 0 N and 0.4 N, as indicated in the introduction.

$$C_0 = \frac{1}{2 \cdot \pi \cdot f_{min} \cdot |Z_{in,f_{min}}|} \tag{1}$$

$$C_m = \frac{C_0 \cdot \Delta f \cdot (\Delta f + 2 \cdot f_0) \cdot (\frac{1}{2 \cdot \pi \cdot i \cdot C_0 \cdot Z_{in,f_0}} - f_0) \cdot (\frac{1}{2 \cdot \pi \cdot i \cdot C_0 \cdot Z_{in,f_0 + \Delta f}} - \Delta f - f_0)}{f_0^2 \cdot (\Delta f + f_0) \cdot (\frac{Z_{in,f_0} - Z_{in,f_0 + \Delta f}}{2 \cdot \pi \cdot i \cdot C_0 \cdot Z_{in,f_0} \cdot Z_{in,f_0 + \Delta f}} - \Delta f)} \tag{2}$$

$$L_m = \frac{(\Delta f + f_0) \cdot (Z_{in,f_0} - Z_{in,f_0 + \Delta f} - 2 \cdot \pi \cdot i \cdot C_0 \cdot Z_{in,f_0} \cdot Z_{in,f_0 + \Delta f} \cdot \Delta f)}{4 \cdot \pi^2 \cdot \Delta f \cdot C_0 \cdot Z_{in,f_0 + \Delta f} \cdot (\Delta f + 2 \cdot f_0) \cdot (2 \cdot \pi \cdot i \cdot C_0 \cdot Z_{in,f_0} \cdot f_0 - 1) \cdot (\Delta f + f_0 - \frac{1}{2 \cdot \pi \cdot i \cdot C_0 \cdot Z_{in,f_0 + \Delta f}})} \tag{3}$$

$$R_m = \frac{Z_{in,f_0}}{1 - 2 \cdot \pi \cdot i \cdot f_0 \cdot C_0 \cdot Z_{in,f_0}} \tag{4}$$

$$\alpha = \left| \frac{2 \cdot \pi \cdot f_0 \cdot \hat{d}_{f_0} \cdot (R_m + 2 \cdot \pi \cdot i \cdot f_0 \cdot L_m + \frac{1}{2 \cdot \pi \cdot i \cdot f_0 \cdot C_m})}{\hat{U}_{in}} \right| \tag{5}$$

Box I.

3.4. Mathematical modeling

As illustrated in Fig. 4, the following procedure is used to derive an extended BVD model, in which the electrical equivalent circuit parameters vary with driving voltage amplitude and force applied at the tip of the transducer using a physical calculus model.

1. Key parameters at mechanical resonance (Fig. 4(b)) are extracted from frequency responses (Fig. 4(a)) at varying operating conditions:

   - f_0: The resonance frequency (frequency of maximal tip displacement amplitude).
   - $\hat{d}_{f_0}$: The amplitude of the displacement of the tip at f_0.
   - $|Z_{in,f_0}|$ and $\angle Z_{in,f_0}$: The magnitude and phase of the input impedance of the transducer at f_0.
   - $|Z_{in,f_{0+\Delta f}}|$ and $\angle Z_{in,f_{0+\Delta f}}$: The magnitude and phase of the input impedance of the transducer at a frequency 10 Hz above f_0.
   - $|Z_{in,f_{min}}|$: The magnitude of the input impedance of the transducer at 27 kHz. This frequency is sufficiently below f_0, such that the influence of the resonance can be neglected.

2. Polynomials are used to approximate the influence of operating conditions on the key parameters (Fig. 4(c)) by minimizing the root mean square error defined by Eq. (10). Polynomials of increasing order are compared to trade-off the complexity and the accuracy of the approximation.

3. Equations for the electrical equivalent circuit parameters C_0, C_m, L_m, R_m, and for the coupling factor α are calculated (Fig. 4(d)) from the approximations of the key parameters using Eqs. (1), (2), (3), (4), and (5) in Box I., which were derived from Eqs. (6), (7), (8), and (9) listed in Appendix.

4. Results

4.1. Influence of driving voltage amplitude

The graph in Fig. 5(a) illustrates the influence of a varying driving voltage amplitude $\hat{U}_{in}$ on the frequency response of the tip displacement and the input impedance of the transducer using Model-A to apply a loading force. The measurements show that an increased driving voltage amplitude results in a stronger tip vibration. The resonance

frequency is reduced with increasing driving voltage amplitude. The magnitude of the input impedance at resonance decreases while the phase of the input impedance at resonance increases with increasing voltage.

4.2. Influence of loading force

Fig. 5(b) illustrates the influence of a varying force applied on the tip of the transducer using Model-A on the frequency responses of the tip displacement and the input impedance of the transducer. An increasing force reduces the displacement of the tip. In contrast to increased voltages, the resonance frequency is increased with increasing force. The magnitude of the input impedance at resonance increases while the phase decreases with increasing force.

4.3. Combined influence of driving voltage amplitude and loading force

The combined influence of driving voltage amplitude and loading force applied using Model-A is depicted in Fig. 6. Empirically we found that the values measured at various forces applied parallel to the main axis of the tip's vibration F_x and perpendicular to the transducer's plane F_y correlate when these two force components are combined as $\bar{F} = F_x + 0.5 \cdot F_y$.

As can be seen in Fig. 6(a), the resonance frequency f_0 decreases with increasing driving voltage amplitude $\hat{U}_{in}$ and increases with increasing force $\bar{F}$.

The influence of load and voltage amplitude on the maximal amplitude of tip displacement is depicted in Fig. 6(b). The displacement amplitude at resonance $\hat{d}_{f_0}$ increases with increasing driving voltage $\hat{U}_{in}$ and is reduced by higher forces $\bar{F}$.

The influence of these operating conditions on the input impedance at resonance is illustrated in Fig. 6(c) and (d). The magnitude of the input impedance at resonance $|Z_{in,f_0}|$ decreases with increasing driving voltage amplitude $\hat{U}_{in}$ and increases with increasing force $\bar{F}$, especially at higher driving voltage amplitudes. The phase of the input impedance at resonance $\angle Z_{in,f_0}$ increases with increasing driving voltage amplitude $\hat{U}_{in}$ and decreases with increasing load $\bar{F}$.

4.4. Influence of calculus hardness

Measurements using Model-B to apply force at the tip of the transducer manifest a similar influence of operating conditions as compared to Model-A.
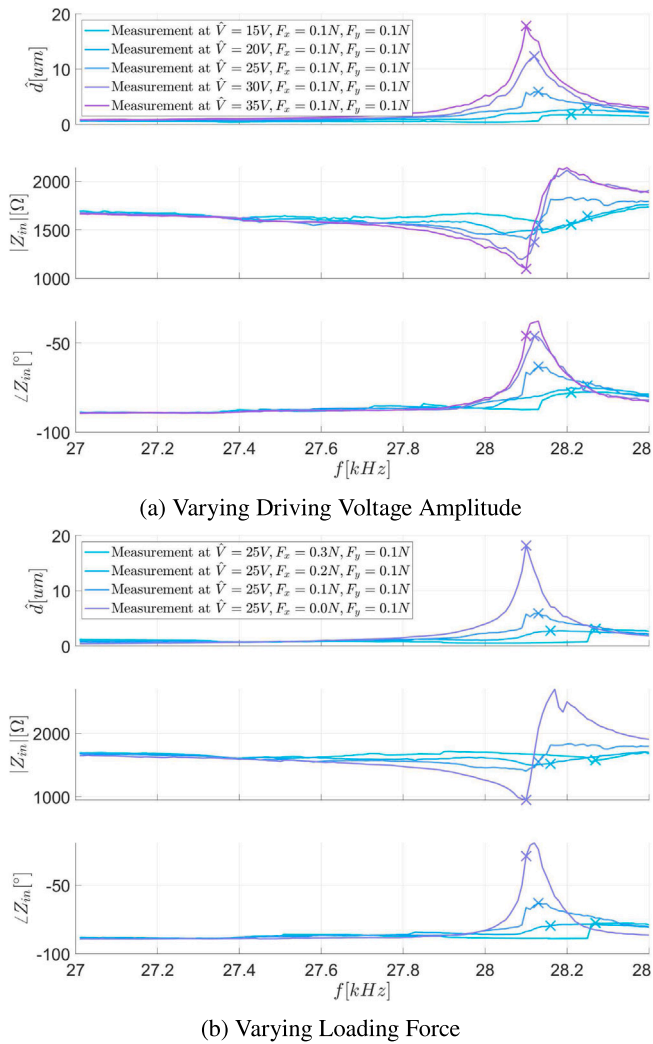
(a) Varying Driving Voltage Amplitude

(b) Varying Loading Force

Fig. 5. Examples of frequency responses of the tip displacement amplitude and the input impedance for varying driving voltage amplitude (a) and for varying force (b) applied using Model-A. Values at resonance are marked with an x.

In particular, an increasing driving voltage amplitude also increases the tip displacement while the resonance frequency is reduced. The magnitude of the input impedance at resonance decreases as well, while the phase of the input impedance increases. However, the reduction of the tip displacement is slightly smaller, while the influence on resonance frequency and the input impedance is more substantial compared to Model-A.

An increasing force applied using Model-B also reduces the tip displacement and the input impedance phase at resonance. In contrast, the resonance frequency and the magnitude of the input impedance at resonance are increased.

4.5. Extended BVD models

The root mean square errors of approximations of the influence of the driving voltage amplitude and the combined loading force applied using Model-A by polynomials of increasing order are listed in Table 1. For the mathematical model polynomials of type P_{13} as defined in Table 2 are selected. These polynomials considerably reduce the root mean square error of $\hat{d}_{f_0}$, $|Z_{in,f_0}|$, $\angle Z_{in,f_0}$, and $\angle Z_{in,f_0+\Delta f}$ as compared to lower order polynomials. Using higher order polynomials is not justified since they only marginally further reduce the error of some values while greatly increasing the computational complexity. The

Table 1
Root mean square error e of approximation of influence of driving voltage amplitude and loading force applied using Model-A on key parameters by polynomials of increasing complexity. Errors of selected polynomials are marked by bold text.

	P_{00}	P_{11}	P_{12}	P_{21}	P_{13}	P_{31}	P_{22}	P_{23}	P_{32}	P_{33}
$e(f_0)$ [Hz]	227	123	117	117	**114**	116	116	111	111	111
$e(\hat{d}_{f_0})$ [µm]	6.58	4.93	3.10	4.18	**2.25**	4.11	3.04	2.09	2.44	2.09
$e(|Z_{in,f_0}|)$ [Ω]	209	162	127	146	**113**	146	127	112	122	112
$e(\angle Z_{in,f_0})$ [°]	17	12	8	11	**6**	11	8	6	7	6
$e(|Z_{in,f_0+\Delta f}|)$ [Ω]	145	123	109	114	**102**	113	109	102	106	101
$e(\angle Z_{in,f_0+\Delta f})$ [°]	18	13	9	12	**7**	12	9	7	8	7
$e(|Z_{in,f_{min}}|)$ [Ω]	29	26	25	26	**24**	25	25	24	24	23

resulting empirically extended BVD model approximating the influence of driving voltage amplitude and loading force applied using Model-A is specified in Table 3.

As illustrated in Fig. 7, these approximations result in a good overall reproduction of the operating conditions' influence on the transducer's characteristics at resonance. As depicted in Fig. 8, the extended BVD model also approximates the influence of the driving voltage amplitude and force on the frequency response of the transducer. While the model generally reproduces the measured values at resonance reasonably well, the reproduction of the magnitude of the input impedance outside resonance is limited. Furthermore, the displacement amplitude considerably differs from the measured values for some combinations of operating conditions.

The resulting extended BVD model approximating the influence of driving voltage amplitude and loading force applied using Model-B is also specified in Table 3.

The extended BVD models allow simulations of the transducer in realistic scenarios, including variations of the driving voltage amplitude, loading force, and hardness of calculus, as illustrated in Fig. 9. As shown in Fig. 9, the extended BVD models reproduce the measured influence of these operating conditions on the resonance frequency, the tip displacement and the input impedance of the transducer, while the standard BVD model does not reproduce these effects.

5. Discussion

5.1. Influence of operating conditions

Applying force using physical models for soft and hard calculus reduces the displacement of the tip and increases the resonance frequency. Additionally, the magnitude of the input impedance at resonance is increased, and its phase is reduced.

While a reduction of the displacement amplitude is expected when a force is applied at the tip of the transducer, the increase in the resonance frequency is not apparent. However, this effect is in agreement with other studies in which Langevin transducers were in contact with a comparatively hard material, such as bone or PTFE [21–24].

The increased resonance frequency can most probably be explained by an increased average stiffness when a force is applied to the transducer by hard material [43]. In this case, the tip of the transducer is in contact with the load material during one part of the ultrasonic oscillation, which results in a considerably increased stiffness of the entire system during this phase. Simultaneously, the comparatively hard load material only adds little additional mass that is jointly accelerated during this phase. As the effect of increased stiffness dominates over the effect of additional mass coupled to the system, the resonance frequency increases [43]. Our measurements indicate that hard (Model-A) and comparatively soft artificial calculus (Model-B) both cause this effect.

In addition, contact with dental calculus increases the system's damping, resulting in an increased input impedance magnitude and a decreased phase and displacement amplitude.
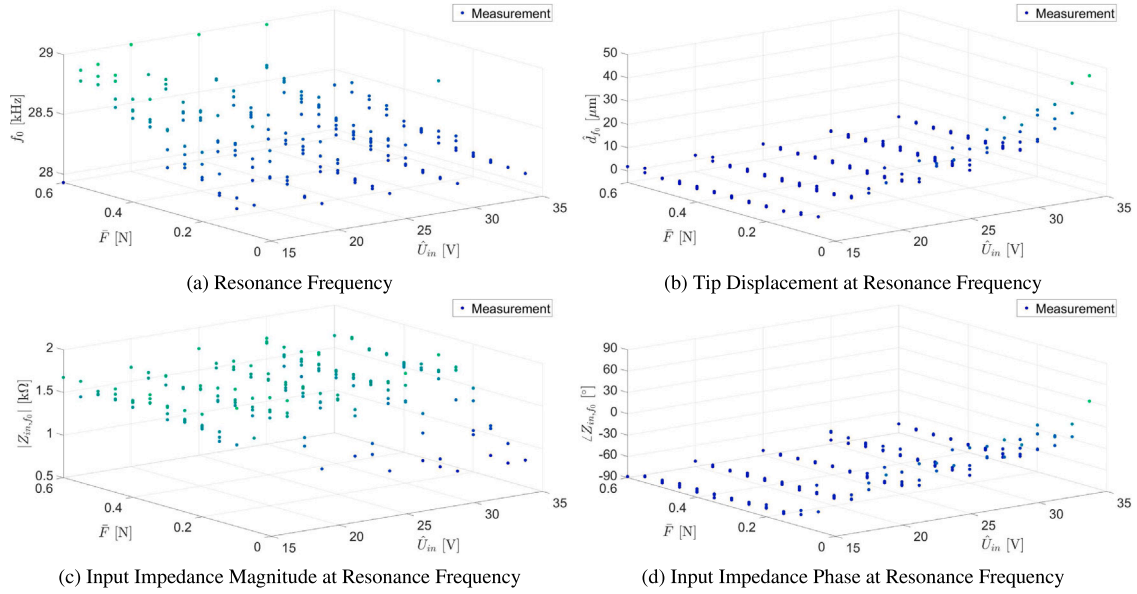
Fig. 6. Measured values of the resonance frequency f_0 (a), the tip displacement amplitude $\hat{d}_{f_0}$ (b), the magnitude $|Z_{in,f_0}|$ (c), and the phase $\angle Z_{in,f_0}$ (d) of the input impedance at resonance for varying driving voltage amplitude and force applied at the tip using Model-A. The components of the force parallel to the main axis of the tip's vibration F_x and perpendicular to the transducer's plane F_y are combined on a single axis $\bar{F} = F_x + 0.5 \cdot F_y$.
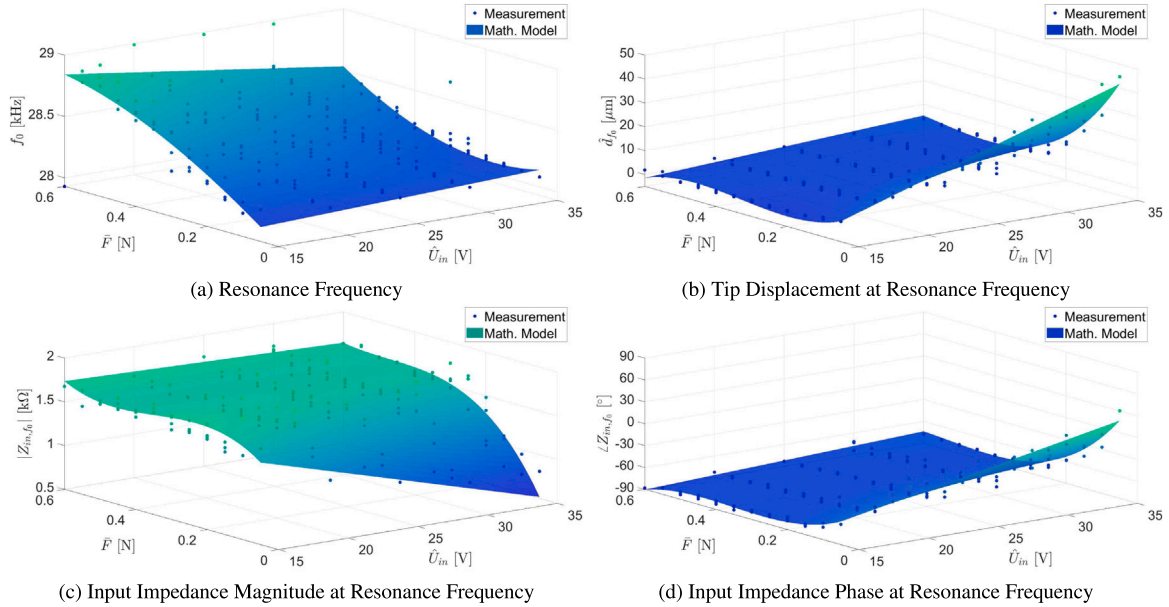

Fig. 7. Approximation of the influence of driving voltage amplitude and force applied at the tip using Model-A on the resonance frequency f_0 (a), the tip displacement amplitude $\hat{d}_{f_0}$ (b), the magnitude $|Z_{in,f_0}|$ (c), and the phase $\angle Z_{in,f_0}$ (d) of the input impedance at resonance by the extended BVD-model defined in Table 3.

Table 2
Polynomials tested to approximate key parameters.

Identifier	Equation
P_{00}	p_{00}
P_{11}	$p_{00} + p_{10}\hat{U}_{in} + p_{01}\bar{F}$
P_{11}	$p_{00} + p_{10}\hat{U}_{in} + p_{01}\bar{F}$
P_{12}	$p_{00} + p_{10}\hat{U}_{in} + p_{01}\bar{F} + p_{11}\hat{U}_{in}\bar{F} + p_{02}\bar{F}^2$
P_{21}	$p_{00} + p_{10}\hat{U}_{in} + p_{01}\bar{F} + p_{20}\hat{U}_{in}^2 + p_{11}\hat{U}_{in}\bar{F}$
P_{13}	$p_{00} + p_{10}\hat{U}_{in} + p_{01}\bar{F} + p_{11}\hat{U}_{in}\bar{F} + p_{02}\bar{F}^2 + p_{12}\hat{U}_{in}\bar{F}^2 + p_{03}\bar{F}^3$
P_{31}	$p_{00} + p_{10}\hat{U}_{in} + p_{01}\bar{F} + p_{20}\hat{U}_{in}^2 + p_{11}\hat{U}_{in}\bar{F} + p_{30}\hat{U}_{in}^3 + p_{21}\hat{U}_{in}^2\bar{F}$
P_{22}	$p_{00} + p_{10}\hat{U}_{in} + p_{01}\bar{F} + p_{20}\hat{U}_{in}^2 + p_{11}\hat{U}_{in}\bar{F} + p_{02}\bar{F}^2$
P_{23}	$p_{00} + p_{10}\hat{U}_{in} + p_{01}\bar{F} + p_{20}\hat{U}_{in}^2 + p_{11}\hat{U}_{in}\bar{F} + p_{02}\bar{F}^2 + p_{21}\hat{U}_{in}^2\bar{F} + p_{12}\hat{U}_{in}\bar{F}^2 + p_{03}\bar{F}^3$
P_{32}	$p_{00} + p_{10}\hat{U}_{in} + p_{01}\bar{F} + p_{20}\hat{U}_{in}^2 + p_{11}\hat{U}_{in}\bar{F} + p_{02}\bar{F}^2 + p_{30}\hat{U}_{in}^3 + p_{21}\hat{U}_{in}^2\bar{F} + p_{12}\hat{U}_{in}\bar{F}^2$
P_{33}	$p_{00} + p_{10}\hat{U}_{in} + p_{01}\bar{F} + p_{20}\hat{U}_{in}^2 + p_{11}\hat{U}_{in}\bar{F} + p_{02}\bar{F}^2 + p_{30}\hat{U}_{in}^3 + p_{21}\hat{U}_{in}^2\bar{F} + p_{12}\hat{U}_{in}\bar{F}^2 + p_{03}\bar{F}^3$

(a) Varying Driving Voltage Amplitude
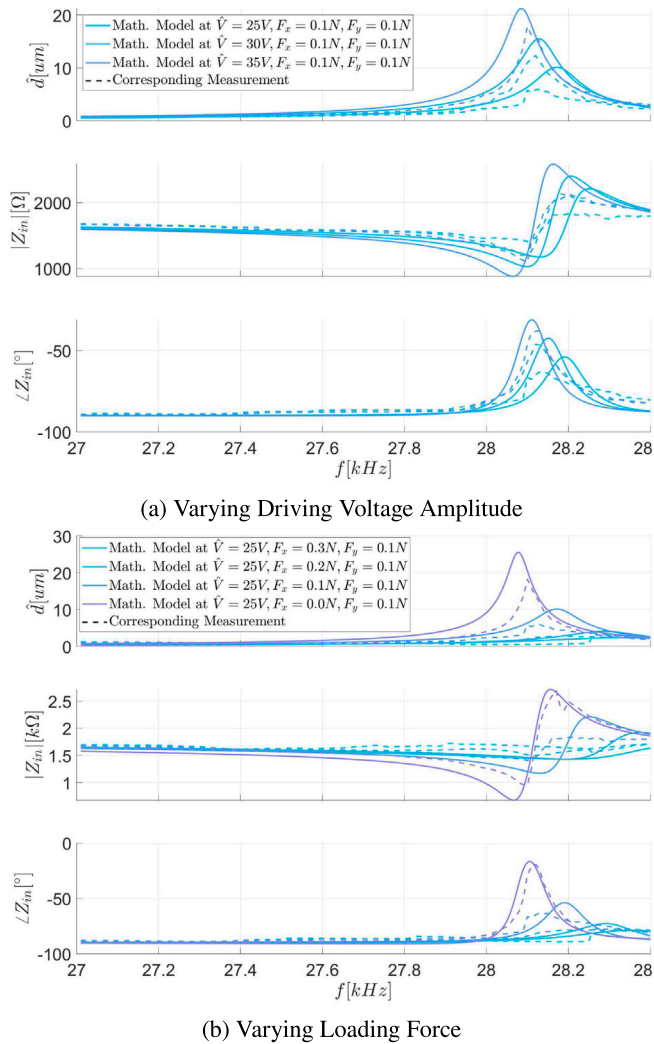

(b) Varying Loading Force

Fig. 8. Simulation of the tip displacement amplitude and the input impedance compared to measured frequency responses for varying driving voltage amplitude (a) and for varying force (b) applied using Model-A.
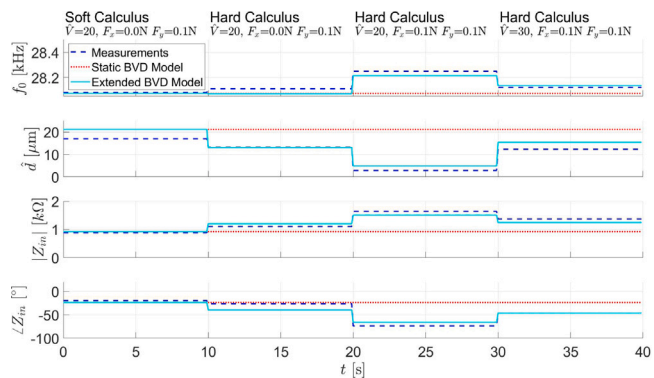

Fig. 9. Results of measurements in comparison to simulations obtained using a static BVD model and using the extended BVD models in a scenario where driving voltage amplitude, loading force, and calculus hardness vary over time.

In contrast to loading force, increasing the driving voltage amplitude has opposite effects on the transducer's characteristics. Increasing the voltage amplitude increases the displacement of the tip and reduces the resonance frequency. The magnitude of the input impedance

at resonance is reduced while its phase is increased. S. Bussier observed the same behavior on a periodontal scaler based on a Langevin transducer [25].

5.2. Mathematical models

Compared to the standard BVD model, the empirically extended BVD models considerably improve the reproduction of the transducer's characteristics. They allow to take variations of the driving voltage amplitude, loading force, and hardness of calculus into account, as depicted in Fig. 9. The extended BVD models reproduce the influence of driving voltage amplitude and load on the resonance frequency, the displacement amplitude, and the input impedance at resonance with sufficient accuracy to facilitate the development of control systems.

The approach to extend the BVD model by approximating key parameters of the transducer's main characteristics by polynomials is simple and straightforward and can be applied to other transducers or extended to other operating conditions.

Even more important, the polynomials used to approximate the key parameters require a comparatively low computational effort compared to equations to calculate them from electrical equivalent parameters. Most feedback control systems for ultrasonic transducers require calculation or estimation of the resonance frequency, tip displacement, and input impedance and can thus be simulated efficiently using such a model.

Last but not least, the presented approach allows to trade off the accuracy and the complexity of the resulting model for different applications. To test the robustness of a control algorithm in the presence of variations of load, linear approximations of the influence of the key parameters may be sufficient. On the other hand, control algorithms that integrate a plant model may profit from approximations using higher order polynomials.

At high loading forces and low driving voltage amplitudes, a discrepancy between the measured frequency response and the frequency response of BVD models emerges, as can be seen in Figs. 5 and 8. Under these conditions, the measurements of the displacement amplitude and the input impedance become increasingly asymmetric with respect to the resonance frequency. Below resonance frequency, the displacement amplitude and the phase of the input impedance are considerably lower than a BVD model predicts. Near resonance, both suddenly increase, and above resonance, they do not decay as fast as predicted by a BVD model.

This asymmetry can most probably be explained by the change of stiffness during the ultrasonic oscillation when the tip touches the loading material, as outlined by C. Duan et al. [44] and C. Comi et al. [45]. As shown by B. D. Yang et al. nonlinear effects of the friction between the tip and the physical calculus model may additionally contribute to the effect [46]. Thus, the extended BVD models' accuracy is limited, especially outside resonance and at low voltage amplitudes and high loading forces.

However, since feedback controllers for ultrasonic scalers track the resonance frequency [10–20] accuracy of the model outside resonance is rarely critical. Furthermore, manufacturing tolerances also cause considerable variations in the characteristics of individual transducer instances, such that control systems must tolerate a certain level of model uncertainties in any case.

5.3. Strength and limitations

As outlined by A. M. Pattison, professionals remove calculus from the edge of the deposit to avoid burnishing the calculus and to remove calculus efficiently [47]. Thus, we adjusted the measurement setup such that the transducer's tip was in contact with the edge of the artificial calculus during the measurements. Nevertheless, due to the elasticity of the transducer's sonotrode and tip, the transducer's tip occasionally slipped onto the surface of the artificial calculus. Therefore we visually

Table 3

Extended BVD-Models when using Model-A and Model-B to apply loading force (coefficients rounded to 3 significant digits).

Symbols:

$\hat{U}_{in}[V]$: Driving voltage amplitude

$F_x[N]$: Force applied parallel to transducer's main axis

$F_y[N]$: Force applied perpendicular to transducer

$\bar{F} = F_x + 0.5 \cdot F_y$: Combined force applied to transducer

$f_0[Hz]$: Mechanical resonance frequency. Frequency of maximal displacement amplitude

$\hat{d}[m]$: Displacement amplitude

$Z_{in}[\Omega]$: Complex input impedance of transducer

Approximation of key parameters for contact with Model-A (hard calculus):

$f_0 = 4750.0 \cdot \bar{F} + 12.3 \cdot \hat{U}_{in} - 165 \cdot \bar{F} \cdot \hat{U}_{in} + 198 \cdot \bar{F}^2 \cdot \hat{U}_{in} - 3940 \cdot \bar{F}^2 - 498 \cdot \bar{F}^3 + 2.78 \cdot 10^{-6}$

$\hat{d}_{f_0} = 6.89 \cdot 10^{-6} \cdot \bar{F} + 2.44 \cdot 10^{-6} \cdot \hat{U}_{in} - 1.12 \cdot 10^{-6} \cdot \bar{F} \cdot \hat{U}_{in} + 1.28 \cdot 10^{-6} \cdot \bar{F}^2 \cdot \hat{U}_{in} + 1.65 \cdot 10^{-6} \cdot \bar{F}^2 - 3.62 \cdot 10^{-6} \cdot \bar{F}^3 - 2.9 \cdot 10^{-6}$

$|Z_{in,f_0}| = 706 \cdot \bar{F} - 57.8 \cdot \hat{U}_{in} + 250 \cdot \bar{F} \cdot \hat{U}_{in} - 269 \cdot \bar{F}^2 \cdot \hat{U}_{in} - 1.04 \cdot 10^{-6} \cdot \bar{F}^2 + 1.4 \cdot 10^{-6} \cdot \bar{F}^3 + 2110$

$\angle Z_{in,f_0} = 0.0844 \cdot \hat{U}_{in} - 0.295 \cdot \bar{F} - 0.402 \cdot \bar{F} \cdot \hat{U}_{in} + 0.476 \cdot \bar{F}^2 \cdot \hat{U}_{in} + 11.9 \cdot \bar{F}^2 - 18 \cdot \bar{F}^3 - 2.02$

$|Z_{in,f_0+\Delta f}| = 68.9 \cdot \bar{F} - 37.5 \cdot \hat{U}_{in} + 163 \cdot \bar{F} \cdot \hat{U}_{in} - 177 \cdot \bar{F}^2 \cdot \hat{U}_{in} - 6470 \cdot \bar{F}^2 + 9460 \cdot \bar{F}^3 + 2040$

$\angle Z_{in,f_0+\Delta f} = 0.092 \cdot \hat{U}_{in} - 0.227 \cdot \bar{F} - 0.426 \cdot \bar{F} \cdot \hat{U}_{in} + 0.491 \cdot \bar{F}^2 \cdot \hat{U}_{in} + 12.3 \cdot \bar{F}^2 - 18.3 \cdot \bar{F}^3 - 2.11$

$|Z_{in,f_{min}}| = 427 \cdot \bar{F} - 2.78 \cdot \hat{U}_{in} + 8.79 \cdot \bar{F} \cdot \hat{U}_{in} - 4.87 \cdot \bar{F}^2 \cdot \hat{U}_{in} - 1940 \cdot \bar{F}^2 + 1730 \cdot \bar{F}^3 + 1690$

Approximation of key parameters for contact with Model-B (soft calculus):

$f_0 = 4530 \cdot \bar{F} - 2.97 \cdot \hat{U}_{in} - 13.8 \cdot \bar{F} \cdot \hat{U}_{in} + 24 \cdot \bar{F}^2 \cdot \hat{U}_{in} - 8880 \cdot \bar{F}^2 + 5470 \cdot \bar{F}^3 + 2.79 \cdot 10^{-6}$

$\hat{d}_{f_0} = 2.57 \cdot 10^{-6} \cdot \hat{U}_{in} - 2.85 \cdot 10^{-6} \cdot \bar{F} - 1.38 \cdot 10^{-6} \cdot \bar{F} \cdot \hat{U}_{in} + 1.64 \cdot 10^{-6} \cdot \bar{F}^2 \cdot \hat{U}_{in} + 5.48 \cdot 10^{-6} \cdot \bar{F}^2 - 7.56 \cdot 10^{-6} \cdot \bar{F}^3 - 1.71 \cdot 10^{-6}$

$|Z_{in,f_0}| = 4280 \cdot \bar{F} - 35.5 \cdot \hat{U}_{in} + 254 \cdot \bar{F} \cdot \hat{U}_{in} - 290 \cdot \bar{F}^2 \cdot \hat{U}_{in} - 1.86 \cdot 10^{-6} \cdot \bar{F}^2 + 1.94 \cdot 10^{-6} \cdot \bar{F}^3 + 1220$

$\angle Z_{in,f_0} = 0.0574 \cdot \hat{U}_{in} - 6.28 \cdot \bar{F} - 0.39 \cdot \bar{F} \cdot \hat{U}_{in} + 0.433 \cdot \bar{F}^2 \cdot \hat{U}_{in} + 34.6 \cdot \bar{F}^2 - 38.1 \cdot \bar{F}^3 - 0.963$

$|Z_{in,f_0+\Delta f}| = 3300 \cdot \bar{F} - 12.1 \cdot \hat{U}_{in} + 95.2 \cdot \bar{F} \cdot \hat{U}_{in} - 98.4 \cdot \bar{F}^2 \cdot \hat{U}_{in} - 9710 \cdot \bar{F}^2 + 8290 \cdot \bar{F}^3 + 1210$

$\angle Z_{in,f_0+\Delta f} = 0.0798 \cdot \hat{U}_{in} - 6.79 \cdot \bar{F} - 0.508 \cdot \bar{F} \cdot \hat{U}_{in} + 0.565 \cdot \bar{F}^2 \cdot \hat{U}_{in} + 40 \cdot \bar{F}^2 - 44.8 \cdot \bar{F}^3 - 1.11$

$|Z_{in,f_{min}}| = 14.7 \cdot \bar{F} \cdot \hat{U}_{in} - 2.14 \cdot \hat{U}_{in} - 434 \cdot \bar{F} - 20.8 \cdot \bar{F}^2 \cdot \hat{U}_{in} + 1250 \cdot \bar{F}^2 - 853 \cdot \bar{F}^3 + 1720$

Calculation of BVD-Model parameters (Note: C_m, L_m, and R_m are complex numbers):

$f_{min} = 27 kHz$

$\Delta f = 10\ Hz$

$Z_0 := |Z_{in,f_0}| \cdot e^{i \cdot \angle Z_{in,f_0}}$

$Z_1 := |Z_{in,f_0+\Delta f}| \cdot e^{i \cdot \angle Z_{in,f_0+\Delta f}}$

$C_0 = \frac{1}{2\pi f_{min}|Z_{in,f_{min}}|}$

$C_m = \frac{C_0 \cdot \Delta f \cdot (\Delta f + 2 \cdot f_0) \cdot \left(\frac{1}{2\cdot\pi\cdot i \cdot C_0 \cdot Z_0} - f_0\right) \cdot \left(\frac{1}{2\cdot\pi\cdot i \cdot C_0 \cdot Z_1} - \Delta f - f_0\right)}{f_0^2 \cdot (\Delta f + f_0) \cdot \left(\frac{Z_0 - Z_1}{2\cdot\pi\cdot i \cdot C_0 \cdot Z_0 \cdot Z_1} - \Delta f\right)}$

$L_m = \frac{(\Delta f + f_0) \cdot (Z_0 - Z_1 - 2 \cdot \pi \cdot i \cdot C_0 \cdot Z_0 \cdot Z_1 \cdot \Delta f)}{4 \cdot \pi^2 \cdot \Delta f \cdot C_0 \cdot Z_1 \cdot (\Delta f + 2 \cdot f_0) \cdot (2 \cdot \pi \cdot i \cdot C_0 \cdot Z_0 \cdot f_0 - 1) \cdot \left(\Delta f + f_0 - \frac{1}{2\cdot\pi\cdot i \cdot C_0 \cdot Z_1}\right)}$

$R_m = \frac{Z_0}{1 - 2 \cdot \pi \cdot i \cdot f_0 \cdot C_0 \cdot Z_0}$

$\alpha = \left| \frac{2 \cdot \pi \cdot f_0 \cdot \hat{d}_{f_0} \cdot \left(R_m + 2 \cdot \pi \cdot i \cdot f_0 \cdot L_m + \frac{1}{2\cdot\pi\cdot i \cdot f_0 \cdot C_m}\right)}{\hat{U}_{in}} \right|$

monitored the position of the transducer's tip relative to the edge of the artificial calculus and repeated measurements if necessary.

During the measurements, artificial calculus was removed. Thus, it was necessary to continuously adjust the position of the physical calculus model to maintain the desired force. This limited the precision of the measurements and the range of forces and driving voltages that could be applied, especially when the comparatively soft Model-B was used as load.

However, due to the large number of measurements and since the effects we observed are strong enough, they can clearly be identified and quantified nonetheless, as documented in Section 4.

To validate the advantages of the extended BVD models, we plan to develop and test a dedicated control system based on these models. Furthermore, we plan to develop a procedure to estimate the force applied at the tip of the transducer and, eventually, to estimate the hardness of calculus in contact with the tip.

6. Conclusion

This study comprehensively analyzed the influence of driving voltage amplitude and load on a novel planar ultrasonic transducer. Increasing loading force increases the resonance frequency and decreases the tip displacement at resonance. Furthermore, it decreases the phase of the input impedance at resonance and increases its magnitude. Increasing driving voltage amplitude causes opposite effects.

Based on the transducer characterization, extended BVD models were developed. The empirical models reproduce the effects of varying driving voltage amplitude and loading force applied by soft and hard artificial calculus.

The gathered data considerably extends the knowledge about the characteristics of planar ultrasonic piezoelectric transducers. The extended BVD models will facilitate the design and initial parameterization of control systems by means of simulation.

CRediT authorship contribution statement

Diego Stutzer: Conceptualization, Methodology, Software, Validation, Investigation, Formal analysis, Resources, Data curation, Writing – original draft, Writing – review & editing, Visualization. **Martin Hofmann:** Conceptualization, Writing – reviewing. **Dominik Wenger:** Software, Data curation, Writing – reviewing. **Khaled Harmouch:** Resources, Writing – reviewing. **Deirdré Lenoir:** Resources, Writing – reviewing. **Juergen Burger:** Supervision, Writing – reviewing, Funding acquisition. **Thomas Niederhauser:** Supervision, Writing – reviewing, Project administration, Funding acquisition.

Declaration of competing interest

The authors declare that they have no known competing financial interests or personal relationships that could have appeared to influence the work reported in this paper.

Data availability

Data will be made available on request.

Acknowledgments

Appendix

$$C_0 := C_0(\hat{U}_{in}, \bar{F}), \quad C_m := C_m(\hat{U}_{in}, \bar{F}), \quad L_m := L_m(\hat{U}_{in}, \bar{F}),$$
$$R_m := R_m(\hat{U}_{in}, \bar{F}), \quad \alpha := \alpha(\hat{U}_{in}, \bar{F}) \tag{6}$$

$$Z_{in} = \frac{C_m \cdot R_m \cdot f \cdot 2\pi i - 4 \cdot C_m \cdot L_m \cdot f^2 \cdot \pi^2 + 1}{2 \cdot f \cdot \pi \cdot (C_0 \cdot i + C_m \cdot i - 2 \cdot C_0 \cdot C_m \cdot R_m \cdot f \cdot \pi - C_0 \cdot C_m \cdot L_m \cdot f^2 \cdot \pi^2 \cdot 4i)} \tag{7}$$

$$\hat{d} = \frac{\alpha \hat{U}_{in}}{2f\pi|R_m + L_m f 2\pi i - i/(2C_m f \pi)|} \tag{8}$$

$$f_0 = |\frac{1}{2\pi\sqrt{C_m L_m}}| \tag{9}$$

$$e(p) = \sqrt{\frac{1}{N}\sum_{i=1}^{N}(p_{model}(\hat{U}_{in,i}, \bar{F}_i) - p_{meas}(\hat{U}_{in,i}, \bar{F}_i))^2},$$

where N is the number of combinations of voltage amplitudes $\hat{U}_{in}$ and forces $\bar{F}$,

and p denotes the parameter that is evaluated e.g.

the mechanical resonance frequency f_0.

$$\tag{10}$$

References

[1] I. Eke Paul, et al., Prevalence of periodontitis in adults in the United States: 2009 and 2010, J. Dent. Res. 91 (10) (2012) 914–920, http://dx.doi.org/10.1177/0022034512457373.

[2] Lewis Winning, Gerard J. Linden, Periodontitis and systemic disease, Bdj Team 2 (2015) 15163, http://dx.doi.org/10.1038/bdjteam.2015.163.

[3] T. Arabaci, Y. Cicek, C.F. Canakci, Sonic and ultrasonic scalers in periodontal treatment: A review, Int. J. Dental Hyg. 5 (1) (2007) 2–12, http://dx.doi.org/10.1111/j.1601-5037.2007.00217.x.

[4] Amit Lal, Richard M. White, Silicon microfabricated horns for power ultrasonics, Sensors Actuators A 54 (1–3) (1996) 542–546, http://dx.doi.org/10.1016/S0924-4247(97)80011-8.

[5] A. Lal, R.M. White, Silicon micromachined ultrasonic micro-cutter, in: 1994 Proceedings of IEEE Ultrasonics Symposium, Vol. 3, IEEE, 1994, http://dx.doi.org/10.1109/ULTSYM.1994.401964.

[6] R. Lockhart, et al., Silicon micromachined ultrasonic scalpel for the dissection and coagulation of tissue, Biomed. Microdevices 17 (4) (2015) 1–12, http://dx.doi.org/10.1007/s10544-015-9981-6.

[7] Martin Hofmann, et al., Development and evaluation of a titanium-based planar ultrasonic scalpel for precision surgery, Available at SSRN 4117191, http://dx.doi.org/10.2139/ssrn.4117191.

[8] Martin Hofmann, et al., Tool tip, tool for dental treatment having such a tool tip and method for operating such a tool. 24.03.2022. European Patent EP3970654A1 https://patents.google.com/patent/EP3970654A1/en.

[9] Martin Hofmann, et al., Finite element modelling for the development of a planar ultrasonic dental scaler for prophylactic and periodontal care, in: International Conference on Modeling Smart Actuators and Piezoelectric Actuators, ICMSAPA, 2022.

[10] Chunsheng Zhao, Ultrasonic Motors: Technologies and Applications, Springer Science & Business Media, ISBN: 978-3-642-15305-1, 2011.

[11] S. Mojrzisch, I. Ille, J. Twiefel, Driving methods and control design for high power ultrasonic transducers, in: International Workshop on Piezoelectric Materials and Applications, IWPMA, 2012.

[12] Y. Kuang, et al., Resonance tracking and vibration stabllization for high power ultrasonic transducers, Ultrasonics 54 (1) (2014) 187–194, http://dx.doi.org/10.1016/j.ultras.2013.07.001.

[13] Masaya Takasaki, Yutaka Maruyama, Takeshi Mizuno, Resonance frequency tracing system for Langevin type ultrasonic transducers, in: 2007 International Conference on Mechatronics and Automation, IEEE, 2007, http://dx.doi.org/10.1109/ICMA.2007.4304183.

[14] Walter Littmann, et al., Load-adaptive phase-controller for resonant driven piezoelectric devices, in: World Congress Ultrasonics, Paris, Vol. 48, 2003.

[15] Smith L. Jack, Use of phase-locked-loop control for driving ultrasonic transducers, 1966, No. NASA-TN-D-3567.

[16] C. Gokcek, Tracking the resonance frequency of a series RLC circuit using a phase locked loop, in: Proceedings of 2003 IEEE Conference on Control Applications, 2003, Vol. 1, CCA 2003, IEEE, 2003, http://dx.doi.org/10.1109/CCA.2003.1223506.

[17] A. Ramos-Fernandez, J.A. Gallego-Juarez, F. Montoya-Vitini, Automatic system for dynamic control of resonance in high power and high Q ultrasonic transducers, Ultrasonics 23 (4) (1985) 151–156, http://dx.doi.org/10.1016/0041-624X(85)90023-X.

[18] Xiaosen Liu, et al., An automatic resonance tracking scheme with maximum power transfer for piezoelectric transducers, IEEE Trans. Ind. Electron. 62 (11) (2015) 7136–7145, http://dx.doi.org/10.1109/TIE.2015.2436874.

[19] B. Mortimer, et al., High power resonant tracking amplifier using admittance locking, Ultrasonics 39 (4) (2001) 257–261, http://dx.doi.org/10.1016/S0041-624X(01)00060-9.

[20] Jack Aldrich, et al., Extremum-seeking control for an ultrasonic/sonic driller/corer (USDC) driven at high power, in: Smart Structures and Materials 2006: Modeling, Signal Processing, and Control, Vol. 6166, SPIE, 2006, http://dx.doi.org/10.1117/12.658872.

[21] Chen Ying, Zhou Zhaoying, Zhang Ganghua, Effects of different tissue loads on high power ultrasonic surgery scalpel, Ultrasound Med. Biol. 32 (3) (2006) 415–420, http://dx.doi.org/10.1016/j.ultrasmedbio.2005.12.012.

[22] Jian-Guo Zhang, et al., Electromechanical dynamics model of ultrasonic transducer in ultrasonic machining based on equivalent circuit approach, Sensors 19 (6) (2019) 1405, http://dx.doi.org/10.3390/s19061405.

[23] Robert William Sutliff, The Effects of Loading on Equivalent Electric Circuit Models for Piezoelectric Transducers, Diss. Miami University, 2018, http://orcid.org/0000-0001-8247-2244.

[24] Lin Shuyu, Load characteristics of high power sandwich piezoelectric ultrasonic transducers, Ultrasonics 43 (5) (2005) 365–373, http://dx.doi.org/10.1016/j.ultras.2004.07.008.

[25] S. Bussier, System Identification for Piezoelectric Transducer Modelling in Dental Application (Master Thesis), Swiss Federal Institute of Technology EPFL, 2017.

[26] Martin Ruppert, et al., In vivo ultrasonic debridement force in bicuspids: A pilot study, J. Periodontol. 73 (4) (2002) 418–422, http://dx.doi.org/10.1902/jop.2002.73.4.418.

[27] Nobuyoshi Hashimoto, Hideo Kato, Kyohei Matsui, Training of tooth scaling by simulator–development of simulator and investigation of its effectiveness, in: 17th International Conference on Artificial Reality and Telexistence, ICAT 2007, IEEE, 2007, http://dx.doi.org/10.1109/ICAT.2007.36.

[28] Thomas Frank Flemmig, et al., Working parameters of a sonic scaler influencing root substance removal in vitro, Clinical Oral Investigations 1 (2) (1997) 55–60, http://dx.doi.org/10.1007/s007840050011.

[29] D.J. White, et al., Instruments and methods for the quantitative measurement of factors affecting hygienist/dentist efforts during scaling and root planing of the teeth, J. Clin. Dentistry (1996) 32–40, 7.2 Spec No PMID: 9238895.

[30] Yasuo Tajime, Research of tooth scaling – About force removing calculus (in Japanese), J. Odontol. Soc. 40 (3) (1977) 414–429.

[31] Donald J. White, Dental calculus: Recent insights into occurrence, formation, prevention, removal and oral health effects of supragingival and subgingival deposits, Eur. J. Oral. Sci. 105 (5) (1997) 508–522, http://dx.doi.org/10.1111/j.1600-0722.1997.tb00238.x.

[32] Adrian Lussi, et al., Das erosive Potenzial verschiedener Getränke, Speisen und Medikamente, Swiss Dental J. 129 (2019) 479–487.

[33] Trevor L.P. Watts, Edward C. Combe, An estimation of the strength of attachment of subgingival calculus to extracted teeth, J. Clin. Periodontol. 8 (1) (1981) 1–3, http://dx.doi.org/10.1111/j.1600-051X.1981.tb02017.x.

[34] IEEE standard on piezoelectricity, 1987, IEEE/ANSI Std. 176.

[35] Igor Ille, Jens Twiefel, Model-based feedback control of an ultrasonic transducer for ultrasonic assisted turning using a novel digital controller, Physics Procedia 70 (2015) 63–67, http://dx.doi.org/10.1016/j.phpro.2015.08.043.

[36] Jens Twiefel, et al., Digital signal processing for an adaptive phase-locked loop controller, in: Modeling, Signal Processing, and Control for Smart Structures 2008, Vol. 6926, SPIE, 2008, http://dx.doi.org/10.1117/12.776091.

[37] Yang Kuang, et al., Ultrasonic cutting with resonance tracking and vibration stabilization, in: 2012 IEEE International Ultrasonics Symposium, IEEE, 2012, http://dx.doi.org/10.1109/ULTSYM.2012.0210.

[38] P. Schweitzer, et al., Feedback sine wave driver design for ultrasonic transducers, Eur. Phys. J.-Appl. Phys. 47 (1) (2009) http://dx.doi.org/10.1051/epjap:2008181.

[39] Arnab Guha, et al., Simple and ultrafast resonance frequency and dissipation shift measurements using a fixed frequency drive, Sensors Actuators B 281 (2019) 960–970, http://dx.doi.org/10.1016/j.snb.2018.11.052.

[40] Witsarut Sriratana, Riichi Murayama, Lerdlekha Tanachaikhan, Synthesis and analysis of PZT using impedance method of reactance estimation, 2013, http://dx.doi.org/10.4236/ampc.2013.31010.

[41] Introduction to ultrasonic drivers. PiezoDrive, Shortland, NSW 2307, Australia, 2021, https://www.piezodrive.com/ultrasonic-drivers/intro-ultrasonic/.

[42] Husain N. Shekhani, et al., High power characterization of piezoelectric ceramics using the burst/transient method with resonance and antiresonance analysis, J. Am. Ceram. Soc. 100 (3) 998–1010, http://dx.doi.org/10.1111/jace.14580.

[43] Stewart Sherrit, et al., Comparison of the mason and KLM equivalent circuits for piezoelectric resonators in the thickness mode, in: 1999 IEEE Ultrasonics Symposium. Proceedings. International Symposium (Cat. No. 99CH37027), Vol. 2, IEEE, 1999, http://dx.doi.org/10.1109/ULTSYM.1999.849139.

[44] Chengwu Duan, Rajendra Singh, Dynamic analysis of preload nonlinearity in a mechanical oscillator, J. Sound Vib. 301 (3–5) (2007) 963–978, http://dx.doi.org/10.1016/j.jsv.2006.10.042.

[45] Claudia Comi, Valentina Zega, Alberto Corigliano, Non-linear mechanics in resonant inertial micro sensors, Int. J. Non-Linear Mech. 120 (2020) 103386, http://dx.doi.org/10.1016/j.ijnonlinmec.2019.103386.

[46] B.D. Yang, M.L. Chu, C.H. Menq, Stick–slip–separation analysis and non-linear stiffness and damping characterization of friction contacts having variable normal load, J. Sound Vib. 210 (4) (1998) 461–481, http://dx.doi.org/10.1006/jsvi.1997.1305.

[47] A.M. Pattison, Keys to effective calculus removal, Dimens. Dental Hygiene 9 (10) (2011) 50–53.

Diego Stutzer earned the M.Sc. degree in electrical engineering and information technology at the Swiss Federal Institute of Technology Zürich (ETHZ) in 2007 with a specialization in biomedical technology. Subsequently he worked in various companies on industrial and research projects as a development engineer and head of engineering. Currently he is studying for a PhD at the Graduate School for Cellular and Biomedical Sciences of the University of Bern and the Bern University of Applied Sciences.

Martin Hofmann completed an apprenticeship as an automation technician in 2012 and graduated from the Zurich University of Applied Science with a bachelor's degree in systems engineering in 2016. Martin Hofmann earned this M.Sc. degree in biomedical engineering at the University of Bern and the Bern University of Applied Sciences in 2018 and worked at the University of Applied Sciences Western Switzerland. Currently, he is doing his Ph.D. at the Graduate School for Cellular and Biomedical Sciences of the University of Bern.

Dominik Wenger received the B.Sc. degree in microtechnology and medical technology from the Bern University of Applied Sciences in 2020 with specialization in optics/photonics and robotics. Currently, he is completing the M.Sc. in electrical engineering at the Bern University of Applied Sciences, where he is also working part-time as scientific assistant.

Khaled Harmouch earned the PhD degree in electromechanical engineering technology at the CentraleSupélec/Université Paris-Saclay in 2018 and subsequently worked as an engineer for MVG Microwave Vision Group. Since 2022, he is employed as a research and development engineer at Electro Medical Systems SA, Nyon, Switzerland.

Deirdré Lenoir earned the M.Sc. degree in mechanical engineering at the Swiss Federal Institute of Technology Lausanne (EPFL) in 2015 with a specialization in material sciences. Subsequently she worked as an engineer for Rolex and Montre Breguet SA and as a scientific assistant at the EPFL. Currently she is employed as research and development engineer at Electro Medical Systems SA, Nyon, Switzerland.

Jürgen Burger earned his Master's and PhD degree in physics at the University of Erlangen. Subsequently, he worked for CSEM and Roche Diagnostics before he was appointed Professor for Microtechnology at the Bern University of Applied Sciences. In 2008, he received the venia docendi and in 2014, he was appointed titular professor in Biomedical Engineering at the University of Bern. Currently, Jürgen Burger is professor for Translational Medicine and Entrepreneurship at the Faculty of Medicine, University of Bern and director of the Swiss School for Translational Medicine and Entrepreneurship at sitem-insel AG, Bern.

Thomas Niederhauser earned his Master's and PhD degree in biomedical engineering at the University of Bern in 2009 and 2014, respectively. Subsequently, he worked as a research associate and lecturer at the University Hospital of Bern (Inselspital), and the Bern University of Applied Sciences. In 2018, he was appointed professor for biomedical signal processing and control and is currently also the head of the Institute for Human Centered Engineering at the Bern University of Applied Sciences.